Shock-Unsteadiness Modification Applied to Oblique Shock Wave/ Turbulent Boundary-Layer Interaction

Amjad Ali Pasha[*]
Department of Aerospace Engineering
IIT Bombay, Mumbai-400076, India

Krishnendu Sinha[†]
Department of Aerospace Engineering
IIT Bombay, Mumbai-400076, India

Abstract

Reynolds averaged Navier-Stokes prediction of shock wave turbulent boundary layer interactions can yield significant error in terms of the size of the separation bubble. In many complex interaction cases, this alters the shock structure and the resulting surface properties. Shock-unsteadiness modification of Sinha et. al. (Physics of Fluids, Vol.15, No.8, 2003) has shown potential in improving prediction in compression corner flows. In this paper, the modification is applied in the simulation of oblique shock wave interacting with a turbulent boundary layer. The flow solution obtained using k-ω turbulence model and the implementation of the shock-unsteadiness correction are described in detail. The shock pattern and the surface properties like pressure and skin friction coefficient are compared with experimental data.

Key words : shock wave, turbulent boundary layer, shock-unsteadiness, separation bubble.

Nomenclature

b_1' shock-unsteadiness damping parameter
C_f Skin friction coefficient
k turbulent kinetic energy (TKE)
M_{1n} Upstream Mach number normal to shock
ω specific dissipation rate of TKE
subscripts
0 upstream of interaction
w wall condition
∞ free stream conditions

1. Introduction

Practically many flows are turbulent in nature. In high speed flows shock waves interact with turbulent boundary layer, altering its characteristics and thereby changing surface properties like pressure, skin friction and heat transfer. Some examples of such interactions are in compression corner, oblique shock impingement on a surface, single fin and double fin configurations. In a hypersonic vehicle, shock wave from nose can interact with turbulent boundary layer in the inlet of scramjet engines. Such oblique shock wave turbulent boundary later interaction (OSWTBLI) can significantly effect the flow in the engine inlet and thus degrade its performance. Accurate flow prediction in these interaction regions is therefore important for the design and operation of scramjet engines.

When a shock wave interacts with a boundary layer, the strong adverse pressure across the shock wave can cause the boundary layer to separate. The location and size of the separation bubble has a strong influence on the flow pattern as well as pressure and heat transfer. Pressure increases at separation point and to a larger extent at reattachment. Heat transfer rate and skin friction attain high values at reattachment point. Flow separation and reattachment often generate additional shock waves and expansion regions which interact among themselves to result in a complex flow pattern.

Reynolds averaged Navier-Stokes (RANS) equations are often used to compute shock wave turbulent boundary layer

[*]Research Scholar, email: amjad@aero.iitb.ac.in
[†]Assistant Professor, email: krish@aero.iitb.ac.in

interaction. Compared to experimental data conventional two equation turbulence models generally result in later separation of the boundary layer[1, 6, 5]. They also under predict separation bubble size and over predict the heat transfer rate at reattachment point. Most of these limitations in RANS computations are attributed to fact that the turbulence models do not account for the unsteady nature of these interactions. Sinha et al.[4] identified a damping mechanism caused by the unsteady interaction of turbulent fluctuations with the shock wave. A correction was added to standard two equation turbulence models to account for this damping effect. The shock unsteadiness modification when applied to supersonic flow over compression corner improved the prediction of separation shock location and the resulting pressure distribution[8].

In this paper, we apply the shock unsteadiness correction to the interaction of an oblique shock wave with a turbulent boundary layer. The next section describes the geometry and flow conditions in the test case of Schulein experiments[9]. Next, we present a summary of governing equations and the shock-unsteadiness modification to k-ω model. Then the numerical method and boundary conditions used in the simulations are described. The last section describes the computed results using standard and shock-unsteadiness modified k-ω turbulence models and their comparison with experimental data.

2. Test case

Experiments were performed by Schulein[9] for the oblique shock wave turbulent boundary layer interaction (OSWTBLI) test case. The geometry consists of a flat plate and a shock generator with three different deflection angles 6 deg, 10 deg and 14 deg as in Fig.1a. The inviscid shock from tip of shock generator interacts with the turbulent boundary layer developed over the flat plate. Free stream conditions are $M_\infty = 5$, $T_\infty = 68.33$ K, and $\rho_\infty = 0.20433$ kg/m^3 with unit Reynolds number $Re_{1\infty} = 37 \times 10^6/m$. The plate is maintained under isothermal conditions of 300 K. Initially the experiments were done for flow over flat plate to obtain turbulent boundary layer values like δ, δ^*, θ and C_f at different locations on the plate. Wall data like pressure, skin friction and heat transfer rates were measured in the interaction region.

3. Simulation Methodology

Two-dimensional compressible RANS equations[10] for the mean flow are solved fully coupled with turbulence model equations. Two equation standard k-ω model of Wilcox[11] and the recent shock-unsteadiness corrected k-ω model of Sinha et. al.[4] are used in the simulations. In-house code[7] is based on finite volume formulation of the governing equations. Inviscid fluxes are computed using Steger-Warming low dissipation method of Candler and MacCormack[2]. Viscous fluxes and turbulent source terms are computed using central difference method. The method is second order accurate in spatial co-ordinates. Implicit data parallel line relaxation method of Wright et. al.[3] is used to integrate in time and reach steady state solution.

The computational domain shown in Fig.1b covers the vicinity of the interaction region. It extends 85 mm upstream and 150 mm downstream of the interaction region. In the y-direction, it extends to 44 mm. At the wall isothermal ($T_w = 300$ K), no slip boundary conditions are applied. At the upper surface of domain, post-shock conditions are given and at the exit boundary, the flow variables are extrapolated from the interior. At the inlet a turbulent boundary layer velocity profile is specified, which is obtained from a separate simulations over a flat plate with same free stream and wall boundary conditions as experiment. The inlet profile is modified at the shock entry point to post-shock conditions calculated analytically. Free stream conditions for k-ω turbulence model are : $k_\infty = 0.01\nu_\infty\omega_\infty = 1.87 \times 10^{-3}$ m^2/s^2 and $\omega_\infty = \frac{10u_\infty}{L} = 8.28 \times 10^3\ s^{-1}$, where $L = 1\ m$ is characteristic length of the plate. The boundary conditions at the wall are taken as $k = 0$ and $\omega = \frac{60\nu_w}{\beta \triangle y_1^2}$, where ν_w is kinematic viscosity at the wall, $\beta = 3/40$, and $\triangle y_1$ is the normal distance to the grid point nearest to the wall.

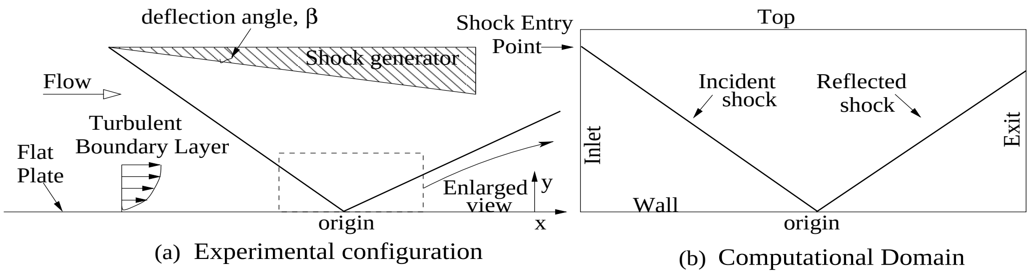

Figure 1: (a) Sketch of experimental configuration with flat plate and shock generator of deflection angle = β deg, depicting oblique shock wave boundary layer interaction (b) The confined part of experiments is taken as computational domain with different boundaries.

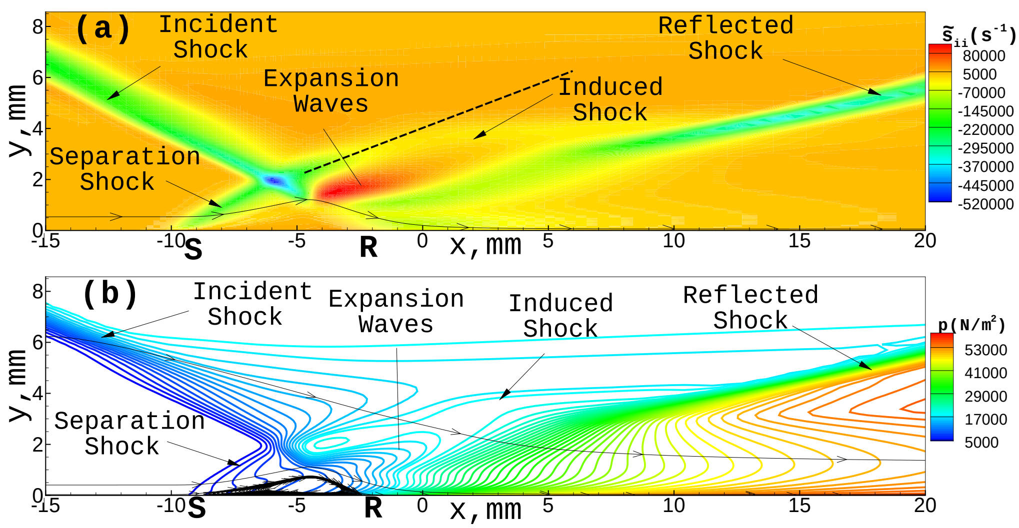

Figure 2: Computations showing dilatation $\tilde{s}_{ii}$ and pressure contours showing different shocks, expansion waves and streamlines with separation bubble, using standard k-ω model for $\beta = 14$ deg and $M_\infty = 5$.

Shock-unsteadiness modified k-ω model

The shock unsteadiness correction[4] is applied by multiplying the eddy viscosity of standard k-ω model by the factor

$$c'_\mu = 1 - f_s[1 + (b'_1/\sqrt{3})/\zeta] \qquad (1)$$

where $\zeta = s/\omega$ is dimensionless mean strain rate, the parameter $s = [2\tilde{s}_{ij}\tilde{s}_{ji} - (2/3)\tilde{s}_{ii}^2]^{1/2}$ and the mean strain rate tensor is $\tilde{s}_{ij} = (1/2)[(\partial\tilde{u}_i/\partial x_j) + (\partial\tilde{u}_j/\partial x_i)]$. The damping parameter b'_1 caused by the interaction of the upstream velocity fluctuations and the shock unsteady motion is given by

$$b'_1 = max[0, 0.4(1 - e^{1-M_{1n}})] \qquad (2)$$

where M_{1n} upstream Mach number normal to the shock wave. The function f_s locates the region of shock wave by the ratio $\tilde{s}_{ii}/s$ and takes the values of one across a shock wave and in other areas it becomes zero. It is defined as

$$f_s = \frac{1}{2} - \frac{1}{2}tanh[8(\tilde{s}_{ii}/s) + 4] \qquad (3)$$

4. Results and Discussions

The oblique shock wave turbulent boundary layer interaction is shown in Fig.2 for a 14 deg shock generator using standard k-ω model. The flow in the interaction region is complex because of the presence of multiple shocks and expansion waves along with flow separation. The dilatation $\tilde{s}_{ii}$ becomes nega-

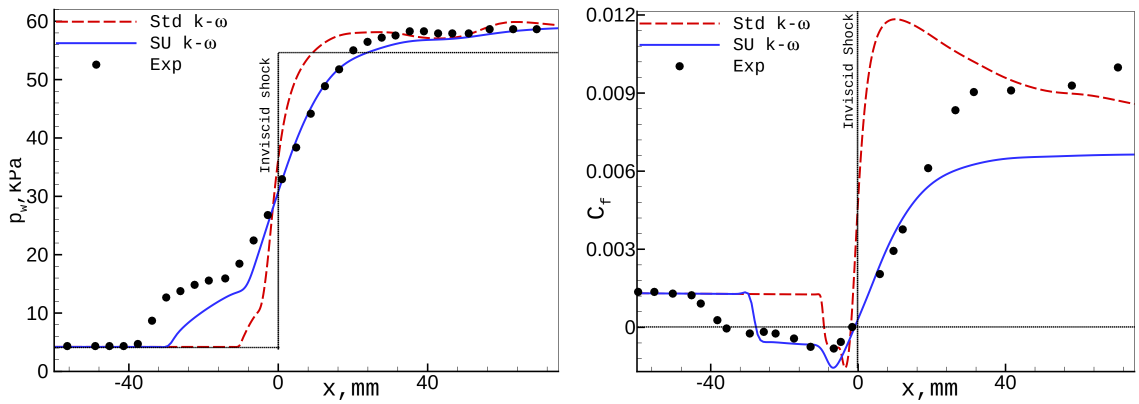

(a) (b)

Figure 3: Computed (a) wall pressure and (b) skin friction with $\beta = 14\,\mathrm{deg}$ using standard (Std) k-ω and modified shock-unsteadiness (SU) k-ω model with $M_\infty = 5$, compared with experiments (Exp).

tive across the highly compressed zones and captures the shock regions accurately. Fig.2b is a magnified view of the interaction region represented by pressure contours. The incident shock interacts with turbulent boundary layer developed over the flat plate causing the flow to separate due to adverse pressure gradient. Streamlines showing the extent of the separation region are plotted where separation (S) and reattachment (R) points are identified. The separation bubble acts as ramp and results in the formation of a separation shock. Intersection of the incident and separation shocks generates an induced shock wave. The intersection point has high flow compression, which is evident from the large negative values of $\tilde{s}_{ii}$ in this region. The flow turns over the separation bubble resulting in the formation of expansion waves. The expansion fan is embedded between induced and reflected shocks and large positive values of dilatation are observed in this region. The expansion waves interact with and weaken the induced shock, which is apparent from low negatives of $\tilde{s}_{ii}$. The expansion waves also cause the induced shock to bend (relative to the dashed line in Fig.2a and merge with the reflected shock formed by the coalescence of compression waves in the reattachment zone. The inviscid flow over the boundary layer is deflected downward through the incident shock. It then passes through induced shock and expansion waves, and finally through the reflected shock to become parallel to the flat plate.

Fig.3(a) shows that variation of pressure and skin friction coefficient along the plate as measured in the experiments. Pressure remains constant in the boundary layer initially up to separation point and rises across the separation shock at x = -36.6 mm. Later it remains approximately constant in the separation bubble, up-to x = -14.2 mm. Flow reattachment causes the pressure to rise to large values and is shown by rapid increase at the end of pressure plateau. Downstream of reattachment pressure remains constant in the recovery region. Due to the adverse pressure gradient across the separation shock the flow separates and C_f crosses zero at x = -33.7 mm. At reattachment point C_f again crosses zero at x = -1.5 mm. In the recirculation zone C_f takes negative values because of flow reversal. In the reattachment region as the boundary layer is compressed, it results in higher velocity gradient and therefore higher C_f. Downstream of the reattachment shock, boundary layer thickness increases hence decreasing C_f for $x >$ 10.5 mm. Simulations show similar trend as experiments but yield a smaller separation bubble (7.4 mm) than experiment (34.1 mm). This results in smaller pressure plateau and a steeper reattachment pressure rise as compared to the measurement. Also, the computed skin friction at reattachment is much higher than experiment.

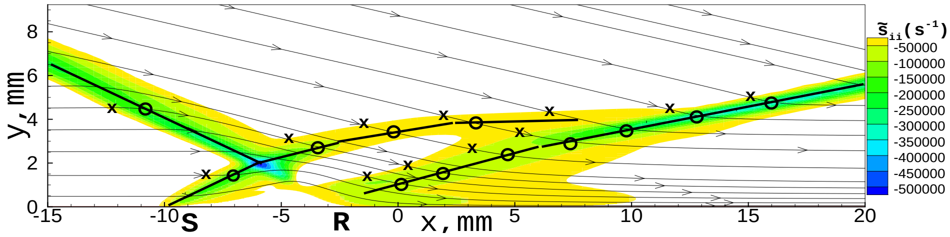

Figure 4: Distribution of $\tilde{s}_{ii}$ depicting different shock regions.Few points depicted by circles are taken on lines (lying on shock regions) and corresponding points upstream of it along the streamline are shown by x.

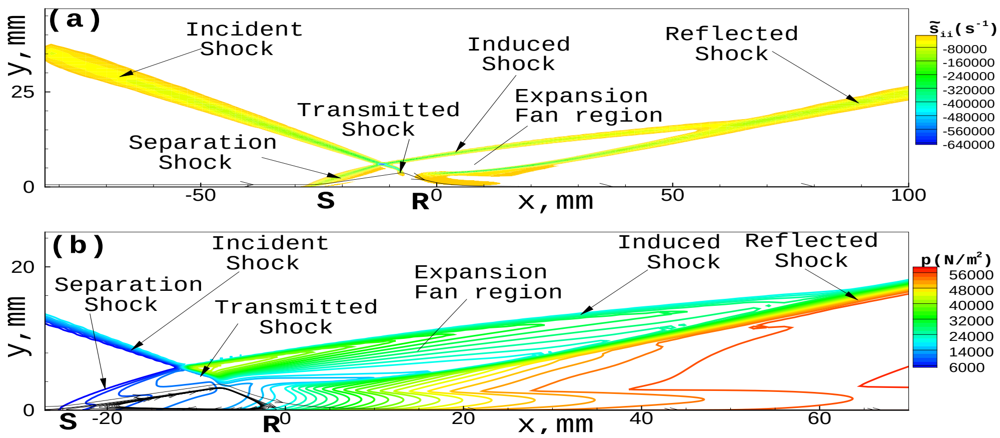

Figure 5: Computations showing dilatation $\tilde{s}_{ii}$ and pressure contours, showing different shocks, expansion waves and streamlines with separation bubble, using shock unsteadiness modified k-ω model for $\beta = 14\,\text{deg}$ and $M_\infty = 5$.

Application of shock-unsteadiness modification

In order to incorporate shock-unsteadiness effects, we need to identify the shock waves and high compression regions in the flow. This is done by the function f_s. To apply the shock unsteadiness modification at a grid point inside a shock we also need to obtain the flow velocity upstream of this location. Then we need to find its component normal to the shock and calculate the corresponding Mach number (M_{1n}). The damping parameter b_1' used in the shock-unsteadiness model is a function of M_{1n}.

The oblique shock wave turbulent boundary layer interaction is a complex zone where the values of upstream Mach number normal to shock M_{1n} has to be determined across the incidence, separation, induced and reflected shock waves shown in Fig.2b. Some of these values depend on the shock pattern in the intersection region and cannot be prescribed a priory. For example, Mach number upstream of reattachment shock depends on the strength of the incident shock, induced shock and expansion waves. For the separation shock upstream Mach number varies approximately between 1.1 to 3.4, and it varies from 3.4 to free stream value of 5 near the boundary layer edge for the incident shock. Downstream of the incident shock wave Mach number decreases to around 3.6 for the induced shock. As the flow expands through expansion waves formed after the induced shock the Mach number varies between 2 to 3.5 upstream of reflected shock wave.

The values of upstream Mach number at different shocks are calculated manually from Fig.4. This is done by taking the angle between the local streamline and the shock wave and using it with the respective upstream Mach number to obtain the Mach number normal to the shock wave M_{1n}. The average value of M_{1n} and b'_1 across the different shock waves in boundary layer region is found to be 1.728 and 1.883 and this value of b'_1 is used to apply the shock-unsteadiness correction.

The shock pattern obtained using shock unsteadiness modification is shown in Fig.5 in terms of dilatation $\tilde{s}_{ii}$ and pressure contours. The shock structure has striking resemblance to the experimental shadowgraph[9]. The high compression (negative $\tilde{s}_{ii}$) regions in Fig.5a match the corresponding dark lines in experimental shadowgraph[9]. These include the incident, separation, induced and transmitted shocks as well as the curve pattern of the reflected shock. The expansion fan generated over the separation bubble curves the induced shock downwards. Similarly the reflected shock is curved upwards by the expansion fan. This effect is clearly seen in Fig.5b.

The main effect of the shock unsteadiness modification is to reduce the amplification of TKE across a shock wave. Lower turbulence results in earlier separation than standard k-ω model and a larger separation bubble is observed. Due to the large separation bubble the shock structure is changed, compared to computations using standard k-ω model. The physics of the formation of different shock waves, expansion waves and recirculation region is similar to the description given in earlier section using standard k-ω model with several differences as described. The large separation bubble causes the separation shock to shift in upstream direction closer to experiments. It also increases the length of the separation bubble and induced shocks. The interaction of incident and separation shock results in transmitted shock. This transmitted shock is very small and is not clear in the k-ω solution. From pressure contour plot of Fig.5b it is observed that the expansion region embedded between induced shock and reflected shock is increased. The induced and reflected shock waves intersect at about 60 mm from origin. In the experiment the expansion fan generated at the end of the shock generator deflects both the induced and reflected shocks upwards. Due to this bending, the two shocks intersect approximately at a distance of 110 mm from the origin. From the shock unsteadiness modified model computations we conclude that the shock structure is improved and shows better prediction in the separation bubble size and separation point location compared with standard k-ω model.

Computed wall pressure and skin friction using shock unsteadiness modified k-ω model are shown Fig.3(a). The standard k-ω model predicts the separation point location far downstream approximately 27.24 mm whereas the shock-unsteadiness modified k-ω model predicts this location 8.1 mm downstream which is closer to experiments. At the separation point the k-ω and modified k-ω model give pressure rise of 2.46 and 3.33 whereas the experiments gives 3.8. The standard model predicts smaller plateau and the modified model yields larger pressure plateau and this is due to prediction of smaller and larger sizes of separation bubble. Later the wall pressure rises in the reattachment region is also better predicted by the shock unsteadiness modification. Computations with k-ω and modified k-ω model give an overall pressure ratio across the separation and reattachment shocks equal to 13.7 and 13.4 which is closer to the experimental value of 13.9. The overall pressure ratio from inviscid theory is calculated as 13.6. The simulations using k-ω model show approximate incident and reflected shock angles to be 24.15 deg and 13.1 deg with respect to wall whereas the inviscid theory gives 23.3 deg and 13.7 deg.

From Fig.3(b) it is observed that C_f remains constant in the boundary layer upstream of the separation shock. It drops before separation point at $x = -10.5$ mm for k-ω model which is at a distance of 34.6 mm downstream of experiments and for the modified k-ω model it drops at $x = -30.6$ mm which is at 14.5 mm downstream. The simulations using modified k-ω model gives larger separation bubble size, equal to 27.1 mm compared to size of 7.4 mm using standard k-ω model. The experiments measure large separation bubble size equal to 34.1 mm. Both the models predict the reattachment point accurately. The k-ω model predicts higher values of C_f across the reattachment region and later drops to near experimental values in the recovery boundary layer. The modified model predicts lower values across the reattachment region and follows the same magnitude in the downstream boundary layer.

5. Conclusions

In this paper, we study the impingement and reflection of an oblique shock wave on a turbulent boundary layer. The configuration chosen is a 14 degree shock generator at Mach 5. Both standard k-ω model and shock-unsteadiness modified k-ω models are used in the simulation, and the results are compared to experimental data. Issues involved in the implementation of the shock-unsteadiness modification are also addressed. These include identification of the different shocks in the numerical solution and calculation of upstream Mach number at each shock location. The standard model yields too small a separation region and hence does not predict the correct shock pattern as seen in the experimental shadowgraphs. The shock-unsteadiness correction yields improved prediction of the separation location as well as the separation bubble size. This in turn results in close matching of the shock structure with the experiment. The surface pressure computed using the modified turbulence model also shows improvement over the standard model.

References

[1] Viegas, J.R., Horstman, C.C., "Comparison of Multi equation Turbulence Models for Several Shock Boundary Interaction Flows", *AIAA Journal*, Vol.17, No.8, pp.811-820, 1979.

[2] MacCormack, R. W., Candler, G.V., Bose, D., "The Solution of Relaxation Methods Using Gauss-Siedal Line Relaxation", *Computers and Fluids*, Vol 17, No. 1, pp. 135-150, 1989.

[3] Wright, M.J., Candler, G.V., Bose, D., "Data-Parallel Relaxation Method for the Navier-Stokes Equations", *AIAA Journal*, Vol 36, No.9, pp. 1603-1609, 1998.

[4] Sinha, K., Mahesh, K., Candler, G.V., "Modeling Shock Unsteadiness in Shock/Turbulence Interaction", *Physics of Fluids*, Vol.15, No.8, pp. 2290-2297, 2003.

[5] Lindbad, I., Wallin, S., Johanson, A., Freiedrich, R., Lechner, R., Krogmann, P., Schulein, E., Courty, J., Ravachol, M., Giordano, D.Sinha, K., Candler, G.V. "Method for High Speed Turbulent Separated Flows with Experimental Verification", *AIAA Paper*, AIAA-98-2547, 1988.

[6] Coakley, T.J., and Huang, P.G., "Turbulence Modeling for High Speed Flows", *AIAA Paper*, 92-0436, 1992.

[7] Sinha, K., Candler, G.V., "Convergence Improvement of Two Equation Turbulence Model Calculations", *AIAA Paper*, 98-2649, June 1998.

[8] Sinha, K., Mahesh, K., Candler, G.V., "Modeling the Effect of Shock-Unsteadiness in Shock/Turbulent Boundary Layer Interactions", *AIAA Journal*, Vol.43, No.3, pp.586-594, 2005.

[9] Schulein, E., "Optical Skin Friction Measurements in Short-duration Facilities", *AIAA Journal*, Vol 44, No.8, pp.1732-1742, 2006.

[10] Wilcox, D. C., "Turbulence modeling for CFD", *DCW Industries*, 2nd ed., 1998.

[11] Wilcox, D.C., "Reassessment of the Scale-Determining Equation for Advanced Turbulence Models", *AIAA Journal*, Vol.26, No.11, pp.1299-1310, 1988.